https://doi.org/10.5194/essd-2024-560
Preprint. Discussion started: 11 December 2024

Open Access Earth System Science Data Discussions

Tracer-based Rapid Anthropogenic Carbon Estimation (TRACE)

Brendan R. Carter[1], Jörg Schwinger[3], Rolf Sonnerup[2], Andrea J. Fassbender[1], Jonathan D. Sharp[2,1], Larissa M. Dias[2,1]

[1]NOAA/OAR Pacific Marine Environmental Laboratory, Seattle, WA, USA
[2]Cooperative Institute for Climate, Ocean, and Ecosystem Studies, University of Washington, Seattle, WA, 98115
[3]Norwegian Research Center, University of Bergen, Nygårdsgaten 112, 5008 Bergen, Norway

Corresponding author address: Brendan.carter@noaa.gov

https://doi.org/10.5194/essd-2024-560
Preprint. Discussion started: 11 December 2024

Open Access Earth System Science Data Discussions

1 Abstract

The ocean is one of the largest sinks for anthropogenic carbon (C_{anth}) and its removal of CO_2 from the atmosphere has been valued at hundreds of billions of US dollars in climate mitigation annually. The ecosystem impacts caused by planet-wide shifts in ocean chemistry resulting from marine C_{anth} accumulation are an active area of research. For these reasons, we need accessible tools to quantify ocean C_{anth} inventories and distributions and to predict how they might evolve in response to future emissions and mitigation activities. Unfortunately, C_{anth} estimation methods are typically only accessible to trained scientists and modelers with access to significant computational resources. Here we make modifications to the transit-time-distribution approach for C_{anth} estimation that render the method more accessible. We also release software called "Tracer-based Rapid Anthropogenic Carbon Estimation version 1" (TRACEv1) that allows users—with one line of code—to obtain C_{anth} and water mass age estimates throughout the global open ocean from user-supplied values of coordinates, salinity, temperature, and the estimate year. We use this code to generate a data product of global gridded open-ocean C_{anth} distributions (TRACEv1_GGC_{anth}, Carter, 2024) that ranges from the preindustrial era through 2500 c.e. under a range of shared socioeconomic pathways (SSPs, or atmospheric CO_2 concentration pathways). We quantify the skill of these estimates by reconstructing C_{anth} in models with known distributions of C_{anth} and transient tracers and by conducting perturbation tests. In the model-based reconstruction test, TRACEv1 reproduces the global ocean C_{anth} inventory with reasonable skill (within ±12 % in 1980 and 2015). We discuss implications of the projected C_{anth} distributions and highlight ways that the estimation strategy might be improved. One finding is that the ocean will continue to increase its net C_{anth} inventory at least through 2500 due to deep ocean ventilation even with the SSP where intense mitigation successfully decreases atmospheric C_{anth} by ~60 % in 2500 relative to the 2024 concentration.

2 Introduction

Humans are emitting ~10 PgC as carbon dioxide gas (CO_2) to the atmosphere every year and a portion of these emissions (~25 %) has entered the ocean (Friedlingstein et al., 2022). Ocean carbon accumulation mitigates global warming by slowing atmospheric CO_2 accumulation. However—in a series of chemical processes known as ocean acidification—the elevated carbon content in seawater also shifts ocean carbonate chemistry toward lower pH and carbonate ion content and toward higher hydrogen ion (H^+) content and CO_2 partial pressure (pCO_2). These chemical shifts have varying and important impacts on marine organisms and potentially on entire ocean ecosystems (Doney et al., 2009, 2020). It is important to be able to distinguish between the large natural background dissolved inorganic carbon (DIC) content and the excess anthropogenic carbon (C_{anth}) present due to human activities if we are to understand the extent, climate impact, and likely future outcomes of ocean C_{anth} accumulation.

Ocean C_{anth} is defined as the difference between the DIC in the modern ocean and the DIC that would be present if humans had never emitted CO_2 (Sabine et al., 2004). It is not a measurable quantity as defined. Without a direct measure, C_{anth} must be estimated, and there are numerous approaches to estimating C_{anth} within the literature including global ocean biogeochemical model (GOBM) simulations (Khatiwala et al., 2013), data-assimilation-based ocean circulation models coupled with air-sea exchange parameterizations (Devries, 2014), approaches that rely on preformed property estimates and remineralization ratios (Vázquez-Rodríguez et al., 2009) or empirical relationships

https://doi.org/10.5194/essd-2024-560
Preprint. Discussion started: 11 December 2024

(Touratier and Goyet, 2004; Yool et al., 2010), comparisons of repeated hydrographic sections (Carter et al., 2019; Gruber et al., 2019b; Müller et al., 2023), techniques such as the transit-time-distribution (TTD) or Green's Function approaches that rely on transient tracers of air-sea exchange to infer histories of atmospheric contact and interior ocean circulation (Khatiwala et al., 2009; Waugh et al., 2006), as well as approaches that combine one or more of these other approaches (Sabine et al., 2004). Isotopic approaches address the related, but not identical, question of "how much of the DIC in seawater is of anthropogenic origin (e.g., Eide et al. 2017)?" Research continues to improve upon these methodologies and to better quantify their uncertainties, often using reconstructions of exactly-known model-simulated C_{anth} distributions (Carter et al., 2019; Clement and Gruber, 2018; He et al., 2018; Matsumoto and Gruber, 2005; Waugh et al., 2006).

While many applications require C_{anth} estimates to be as accurate as possible, other applications are more flexible and limited primarily by C_{anth} estimate (1) accessibility, (2) computational efficiency, and (3) the ability to project the estimate forward or backward in time.

1) Accessibility: Implementation of most C_{anth} estimation strategies requires nuanced understanding of the methodology so that decisions can be made about the parameters used in forward or inverse models or how and whether to account for various biogeochemical processes (e.g., calcification, organic matter ballasting, or iron dynamics and limitation). In addition, many C_{anth} estimation strategies require the presence of collocated high-quality measurements of physical and biogeochemical properties (e.g., empirical multiple linear regression C_{anth} change estimates) or transient tracer content measurements (e.g., TTD or Green's Function based estimates).
2) Computation efficiency: Some C_{anth} estimation strategies require downloading and employing large sparse matrices (Davila et al., 2022) and others require iterative inverse model reconstructions or forward model simulations to be run with GOBMs (DeVries et al., 2017; Khatiwala et al., 2013).
3) Projection: Many C_{anth} estimation techniques are limited to a narrow time window. For example, the "extended multiple linear regression" approaches are usually limited to the period spanned by repeated shipboard hydrographic measurements (Carter et al., 2019; Gruber et al., 2019a; Müller et al., 2023). A related problem is the need to adjust a DIC dataset that was measured across years or decades to be specific to a single reference year or year of interest. To make this adjustment, it is important to know how much the DIC value would have changed due to C_{anth} accumulation between when it was measured and the reference year. Simplistic adjustments invoking transient steady state (Gammon et al., 1982) C_{anth} accumulation are commonly employed (Carter et al., 2021a; Clement and Gruber, 2018; Lauvset et al., 2016; Müller et al., 2023), but are problematic for larger adjustments that are often associated with longer time gaps. An example of an application that faces these challenges is given in Supplementary Text S1.

Here we describe, assess, and present results from a new method that we call "Tracer-based Rapid Anthropogenic Carbon Estimation version 1" or TRACEv1, which aims to provide C_{anth} estimation that meets the previously listed needs without overly compromising on C_{anth} estimate accuracy. TRACEv1 is an approach that retains much of the

https://doi.org/10.5194/essd-2024-560
Preprint. Discussion started: 11 December 2024

skill of the more complex approaches and yet is quick; nearly global; easy to use; computationally efficient; able to generate plausible projections over a limited time horizon; and requires only coordinate information (longitude, latitude, and depth), salinity (S), temperature (T), the desired year for the estimate, and (for projections) the assumed shared-socioeconomic pathway (i.e., SSP, or atmospheric CO_2 concentration over time).

In this manuscript we present three products. The first is the TRACEv1 code itself, which is, initially, released only for the MATLAB computing language, though a Python port is planned. The code contains subroutines that use neural networks to remap the preformed property estimates of Carter et al. (2021b) to the locations and conditions provided by users calling the TRACEv1 routine. The second is an estimate of the likely uncertainties in TRACEv1 estimates based on an analysis of the errors found when the method is trained using transient tracer information extracted from a GOBM simulation—with a spatial and temporal distribution that mirrors the availability of CFC-11, CFC-12, and SF_6 measurements in the real ocean—and is used to reconstruct the exactly-known GOBM C_{anth} distributions. The third is a data product of global C_{anth} from TRACEv1 with varied 10-to-100-year resolution from 1750 through 2500. This product uses a variety of SSPs for projections after 2015.

3 Methods

First, we describe the conceptual framework for TRACEv1 and explain in detail how it works. Then we introduce the observational datasets used to train TRACEv1 and explain how transit time distribution parameters and preformed properties are empirically fit and estimated on demand. Finally, we explain how TRACEv1 is used to generate the TRACEv1_GGC_{anth} product (Carter, 2024).

3.1 Conceptual framework and historical context

TRACEv1 emulates the inverse Gaussian (IG) TTD method for C_{anth} estimation, but with several modifications. Traditionally, the TTD approach makes assumptions about the distribution of ages (length of time since seawater was last in contact with the atmospheric) of the various parcels of seawater that combine to produce the seawater observed in the ocean interior. Assumptions are also needed about the degree of air-sea equilibration with transient tracers. These assumptions are collectively used to tune the age distribution to match transient tracer observations, and then similar assumptions are used to infer the C_{anth} content that would be expected for that mixture of seawater from the distribution of ages and the known history of atmospheric CO_2 accumulation (e.g., He et al. 2018). TRACEv1 also follows these steps. The most important modification is that we reduce the TTD shape to a single term (α), optimize this term to reflect transient tracer and modeled ideal age distributions as normal, and then train a neural network capable of predicting this term using only physical measurements of seawater and coordinate information. This allows us to estimate C_{anth} from a TTD without the need for collocated transient tracer observations at the time and place where the estimate is desired.

When optimizing α, CFC-11, CFC-12, and SF_6 are dominant constraints for younger waters, while water mass ideal ages (A) (Thiele and Sarmiento, 1990)—taken from a model that assimilates transient tracer observations and measurements of the long-lived ^{14}C radionuclide— are primarily included as a constraint for the oldest water masses.

https://doi.org/10.5194/essd-2024-560
Preprint. Discussion started: 11 December 2024

SF_6 measurements are particularly strong constraints for the youngest waters ventilated since the 1990s maxima in CFC-11 and CFC-12 concentrations, but are only available for ~30 % of the measured bottles. All constraints available are used for optimizing all water parcels, and the strong constraint for young (old) waters and weak constraint for old (young) waters provided by transient tracers (A) results naturally due to how the values, their magnitudes, and their misfits vary with the age of the water mass. The transient tracer constraints dominate in younger waters where the transient tracer measurements are largest while the A constraint dominates in water masses that are older than the advent of measurable atmospheric transient tracer concentrations in the 1940-1960s. For water parcels older than ~1940, there is essentially no sensitivity to the transient tracer information. TRACEv1 is therefore more of an observation-based product in the surface ocean and an observation-tuned-model-based product in the deep ocean.

Several recent developments have enabled TRACEv1: First, the training data are taken from the recent 2023 update to the Global Data Analysis Project version 2 (GLODAPv2.2023) data product (Lauvset et al., 2024). This data product contains >270k bottle measurements with both CFC-11 and CFC-12 and >70k more measurements with CFCs and SF_6 measurements (Fig. 1); SF_6 was first included in the 2022 GLODAP release (Lauvset et al., 2022). CFC distributions have long been used to estimate C_{anth}, and oceanographic SF_6 measurements are available from many recent cruises owing to methodological developments by Tanhua et al. (2004) and advances allowing CFC and SF_6 measurements on the same samples (Bullister et al., 2006) implemented by GO-SHIP transient tracer teams globally (Erickson et al., 2023). Second, water mass ideal ages from the recently-released transport matrix solutions of the Ocean Circulation Inverse Model of (John et al., 2020) provide an additional constraint for TRACEv1. TRACEv1 uses a preformed property data product (Carter et al., 2021b) to estimate the composition of seawater when it was last exchanging CO_2 with the atmosphere. Finally, the approach is assessed against newly simulated C_{anth}, CFC, and SF_6 distributions (Müller, 2023) that were generated as part of the second Regional Ocean Carbon Cycle Assessment and Processes effort (RECCAP2, e.g., DeVries et al. 2023). The simulated CFC and SF_6 distributions were not previously published as part of the RECCAP2 data product or used by the analyses.

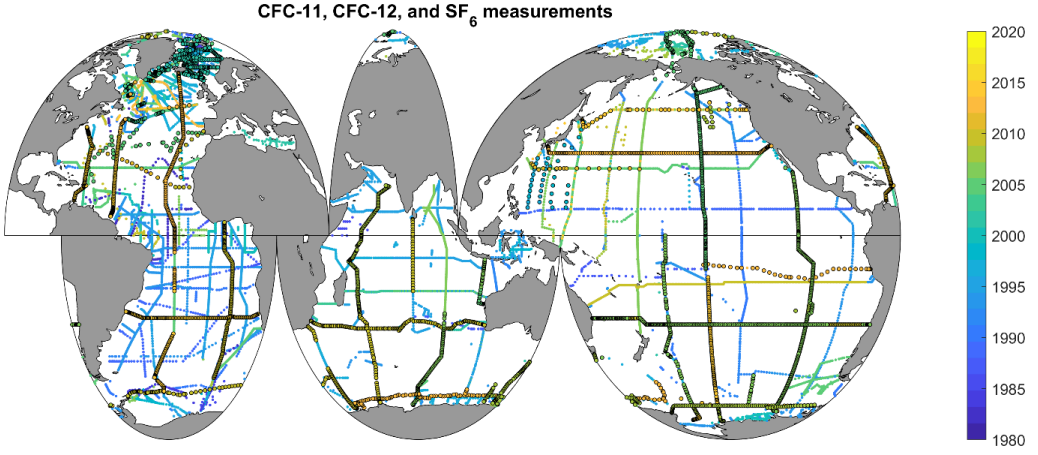

https://doi.org/10.5194/essd-2024-560
Preprint. Discussion started: 11 December 2024

Figure 1. Locations and years of measurements of CFC-11 and CFC-12 in the GLODAPv2.2023 data product (Lauvset et al., 2024). Dark borders around measurements indicate SF_6 is available alongside CFC-11 and CFC12.

3.2 How TRACEv1 works

We begin with a summary of the TRACEv1 functions and then explain the various steps in greater detail: The TRACEv1 code:

1. uses a neural network to estimate an age distribution for seawater from a user-specified location, *T*, and *S*, and returns the mean age if this is a desired output;
2. uses a record or projection of the atmospheric CO_2 in the years leading up to the date of the desired estimate to determine an anthropogenic CO_2 level for each component of the water mass mixture;
3. convolves the age distribution with the component's CO_2 history to estimate a component-fraction-weighted mean atmospheric CO_2 for the water parcel;
4. uses another set of neural networks to estimate the preformed properties of this water mass mixture from the user-specified location, *T*, and *S*;
5. estimates the degree of CO_2 disequilibrium expected for the surface ocean when responding to rapid changes in atmospheric xCO_2;
6. and solves for the C_{anth} distribution as the difference between the total dissolved inorganic carbon (DIC) value that corresponds to the surface ocean equilibration level associated with the transient xCO_2 and the DIC value that corresponds to a "preindustrial" atmospheric xCO_2 of 280 ppm. The TRACEv1 code allows users to substitute arbitrary reference preindustrial xCO_2 values to obtain estimates that are comparable to literature estimates that have used alternative baselines, but all calculations provided herein are obtained using 280 ppm.

Committees of neural networks (henceforth just "neural networks") are used to estimate four pieces of information in a standard TRACEv1 estimate (a fifth neural network is invoked when *T* information is not supplied by the user). The neural networks are similar in construction to those used by the ESPER_NN routines (Carter et al., 2021a), and are described in more detail in Supplementary Text S2. Three of the neural networks estimate preformed biogeochemical properties of the seawater (explained below) and the fourth is a parameter related to the TTD construction called α. A fifth neural network allows *T* to be estimated from *S* if *T* is not provided as a user input (this is not the recommended use of TRACEv1, and is recommended that users who invoke this functionality perform validation of the estimates returned for their purposes and do not rely on the validation provided herein, which is specific to estimates obtained from both *T* and S_J.

Preformed properties are estimates of the properties that interior ocean seawater mixtures had when they last were in contact with the atmosphere near the ocean surface. These are the properties impact air-sea gas exchange equilibrium processes when C_{anth} was last able to change through contact with the atmosphere. In TRACEv1 preformed total titration seawater alkalinity content (TA^0), preformed dissolved inorganic silicate content (Si^0), and preformed

https://doi.org/10.5194/essd-2024-560
Preprint. Discussion started: 11 December 2024

dissolved inorganic phosphate content (P^0) are collectively used with pCO_2 as constraints for the carbonate chemistry of seawater near the sea surface. These three quantities are estimated from three separate neural networks trained using latitude, longitude, depth, *S*, and *T* from the Lauvset et al. (2016) global gridded version of the GLODAPv2 data product as predictor information and the preformed property estimates of Carter et al. (2021b), estimated for the same gridded product, as target/validation data. The uncertainty contribution from errors in preformed properties is a small contributor to the overall C_{anth} uncertainty (Supplementary Text S3).

The fourth neural network estimates α, which is used to construct the TTD. The TTD is an evolution of the "water mass age" concept (Bolin and Rodhe, 1973; Hall and Haine, 2002). While a water mass age is an estimate of the average length of time since a given parcel of interior ocean seawater was last at the ocean surface, a TTD comes from the recognition that interior ocean seawater is better represented as a mixture of many different water parcels—each with a different history of atmospheric contact and interior ocean circulation—than as a single parcel of water with a single *A*. One-dimensional pipe flow with diffusion results in a distribution of ages that can be well approximated using an IG age-fraction distribution (Peacock and Maltrud, 2006; Waugh et al., 2003) and provides good agreement with available transient tracer data (Sonnerup et al., 2013; Stanley et al., 2012; Waugh et al., 2004). However, there are places in the ocean where comparatively "young" (i.e., recently ventilated) waters mix with very old deep waters in appreciable amounts (e.g., Antarctic Intermediate Water, which is formed through the mixing of fresh surface waters near the polar front with upwelling upper circumpolar deep water, see: Naveira Garabato et al., 2009), and in these areas the one-dimensional pipe model age distribution is inadequate (Ito and Wang, 2017; Peacock and Maltrud, 2006). With this and similar concerns driving innovation, many variants on the underlying TTD shape have been used. However, experimentation with these variants did not reveal any meaningful improvement over the simple IG distribution for reconstructing modeled C_{anth} (Hall et al., 2002; Waugh et al., 2003, 2006) so we retain the simple IG formulation. Given the limited number of options tested, it is plausible that alternative age distributions could outperform the distribution fitting terms that we employ for TRACEv1. This is particularly likely for *A* estimates, as erroneous transit time distribution shapes have been shown to be less problematic for C_{anth} than for *A* due to the similarities between the atmospheric growth curves for transient tracers and C_{anth} (Waugh et al., 2006).

The predicted parameter α is used to convert a unitless IG distribution into an age distribution. IG probability distributions for an arbitrary coordinate variable "*x*" are shaped by two parameters "Γ" (mean) and "Δ" (shape parameter). Some consideration has been given in the literature to the ideal values for these parameters for TTD analyses. Based on the results of He et al. (2018), we choose a Γ=1 and Δ=1/1.3 (or ~0.77) and we find in our model-based assessments that this assumption performs equivalently (within uncertainties) to the common alternative assumption of Γ=Δ=1. The standard form of the IG probability distribution with a Γ=1 and Δ=0.77 (Equation 1) is evaluated from x=0.01 to x=5 (by increments of 0.01):

$$f(x) = \sqrt{\frac{0.77}{2\pi x^3}} e^{-\frac{0.77(x-1)^2}{2x}} \quad (1)$$

https://doi.org/10.5194/essd-2024-560
Preprint. Discussion started: 11 December 2024

The α is then used to identify the ages associated with this IG probability distribution, where the age values assigned to the 500 $f(x)$ values equal [1:500]*α years. The resulting age-probability distribution is then interpolated to integer ages for the most recent 1000 years. When α is <2 it becomes impossible to interpolate across all 1000 years, but in these cases the missing values correspond to negligible fractional contributions and are neglected. The sum of these interpolated contributions usually diverges slightly from 1 due to the discretization of the continuous probability distribution and the inability to interpolate to all years, so the non-neglected component fractions are further divided by their sum to ensure they add to unity. Thus, when α is a large number the mean A of the Gaussian distribution is large (Fig. 2) and when α is smaller A is smaller.

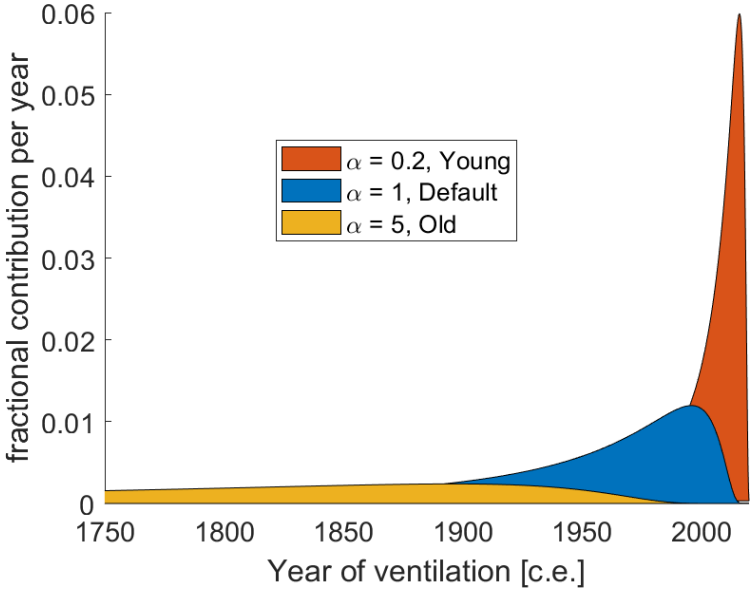

Figure 2. Three example ventilation-year distributions for a parcel of water observed in the year 2020. The "Young," "Default," and "Old" mixtures in orange, blue, and yellow have mean ages of ~17, 91, and 460 years, respectively. Fractions of a given color add up to 1 when summed across all years.

Once the age distribution is known, the atmospheric CO_2 record is convoluted into the age distribution as follows (Hall et al., 2002): First, the atmospheric record or projection is interpolated to obtain values for the year of the desired estimate minus the ages in the distribution. Then for each of the (up to) 1000 fractions of the water mass, the fraction-weighted mean ages ($\bar{A}$) and concentrations ($\overline{[X]}$) can be computed as fraction-weighted sums. E.g. for gas X with atmospheric concentration $[X]$ summed over the i=1:1000 years prior to the estimate of interest this would be computed as:

$$\overline{[X]} = \sum_{i=1}^{1000} f_i [X]_i \quad (2)$$

https://doi.org/10.5194/essd-2024-560
Preprint. Discussion started: 11 December 2024

For the $\bar{A}$ calculation, [X_i] is replaced in this equation with i years. The concentration values reflect complete air-sea equilibration, which is inconsistent with net ocean uptake of CO_2 from air-sea gas exchange. For example, in the Regional Carbon Cycles and Processes model simulations there is a 108 ±4 µatm increase in the surface ocean pCO_2 in 2018 relative to the preindustrial value compared to a 128.72 µatm change in the atmospheric xCO_2 (DeVries et al., 2023; Müller, 2023). Also, the air sea CO_2 disequilibrium is thought to vary temporally (He et al., 2018) and be sensitive to the rate of atmospheric xCO_2 change. We therefore derive an empirical relationship between atmospheric xCO_2 and the median model-observation-hybrid apparent surface ocean pCO_2 record given by Jiang et al. (2023). A variety of predictive relationships were tested, and the strongest predictive relationship (lowest RMSE) was obtained for:

$$pCO_{2,oce.year} = xCO_{2,atm.year} - 0.144 * (xCO_{2,atm.year}\text{-}xCO_{2,atm.year\_minus\_65}) \quad (3)$$

Equation (3) suggests the expected surface ocean pCO_2 value in an arbitrary year $pCO_{2,oce.year}$ can be estimated as a function of the atmospheric xCO_2 in that year ($xCO_{2,atm.year}$) and the difference between that atmospheric value and the value in the atmosphere 65 years prior ($xCO_{2,atm.year\_minus\_65}$). Applying equation (3) to the xCO_2 record before use in TRACEv1 meaningfully reduces the mismatch between the simulated surface ocean pCO_2 and the atmospheric xCO_2 (Fig. 3). An additional constant offset of −5.37 µatm was found in the best fit relationship (not shown on the right side of equation 3), but this term likely reflects the water vapor correction between xCO_2 and pCO_2 and, potentially, parameterized net model degassing of riverine carbon. TRACEv1 neglects this constant offset because the code separately applies the water vapor correction for each parcel of seawater (Dickson et al., 2007) when converting between xCO_2 and pCO_2 and because including this term would have a nearly identical impact on preindustrial pCO_2.

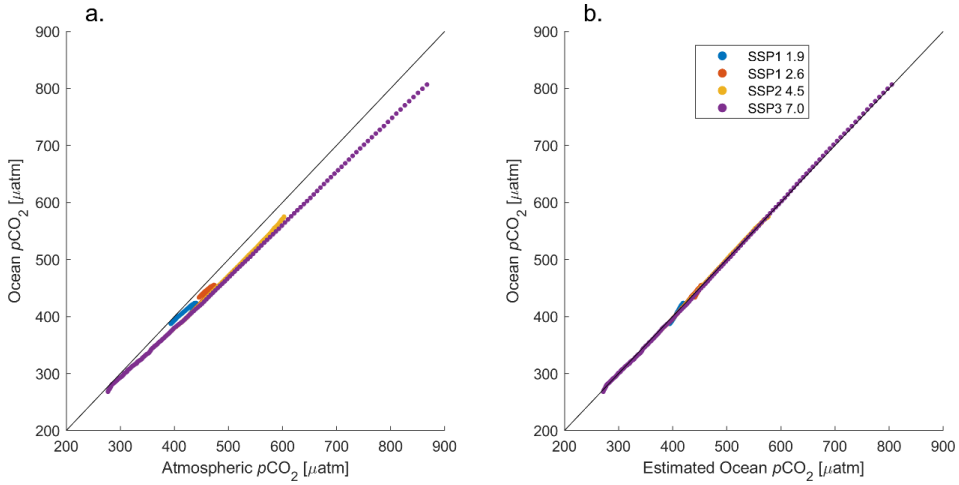

Figure 3. A comparison between surface ocean pCO_2 values in the model-based data product of Jiang et al. (2023) and **(a.)** the modeled atmospheric xCO_2 value and **(b.)** the value obtained from equation (3). Black 1:1 lines are provided for reference, and the colored dots indicate projected and historical values from 4 different SSPs.

https://doi.org/10.5194/essd-2024-560
Preprint. Discussion started: 11 December 2024

Once water-fraction-weighted mean pCO_2 values $\overline{[pCO_2]_{oce.}}$ are estimated for a parcel of seawater, the expected equilibrium DIC value for the water parcel when last at the ocean surface is calculated using estimated TA^0, Si^0, and P^0. These calculations are repeated with both the $\overline{[pCO_2]_{oce.}}$ and a user-provided preindustrial xCO_2 value (default is 280 ppm, adjusted for water vapor), and their difference is attributed to C_{anth}. During fitting of the α values (described later) a similar procedure is followed for transient tracer observations with CFC and SF_6 equilibrium constants (Bullister et al., 2002; Warner and Weiss, 1985), though without adjustments for incomplete equilibration because the equilibrium timescales for these tracers are shorter than for CO_2.

Carbonate chemistry calculations are computed with the CO2SYS code written for MATLAB (Van Heuven et al., 2011) and modified herein to increase the tolerance for pH changes during iteration from 0.0001 to 0.001 when converging on a pH value (to speed up the calculation). Carbonate dissociation constants from Lueker et al. (2000) are used with the total boron calculation from Uppström (1974) and the K_F calculation from Perez and Fraga (1987). S and T values that are outside the viable range for these carbonate chemistry constants (S=19 to 48 and T=2 °C to 35 °C) are overridden with the nearest viable S and T values. This override has a minimal impact on most C_{anth} calculations for common seawater types, but we caution here that TRACEv1 is not intended for use in freshwater or brackish environments. Information on computing optimization is provided in Supplementary Text S4.

3.3 Data and model output used to train and run TRACEv1

The α parameter is fit to the CFC-11, CFC-12, and SF_6 partial pressures that would be found in a gas phase in complete air-sea equilibrium with seawater with the measured composition, as well as to A from the "Ocean Circulation Inverse Model" (OCIM) transport matrix (John et al., 2020) when the zero-age boundary layer is set equal to the shallowest layer in the OCIM model. For the real ocean, the transient tracer partial pressure values are taken as calculated from discrete seawater measurements in the GLODAPv2.2023 data product (Lauvset et al., 2024). Collocated measurements of salinity and temperature are also extracted from this data product. For the model reconstruction test, C_{anth}, S, and T are taken from or computed from the NorESM RECCAP2 simulations (Müller, 2023). In addition to the standard RECCAP2 outputs, this model was also used to simulate CFC-11, CFC-12, and SF_6 through 2015. These fields are made available as Supplementary Data S1. The approaches used to obtain scattered values from gridded model output and to obtain scattered ages from the OCIM transport matrix are given in Supplementary Text S5.

https://doi.org/10.5194/essd-2024-560
Preprint. Discussion started: 11 December 2024

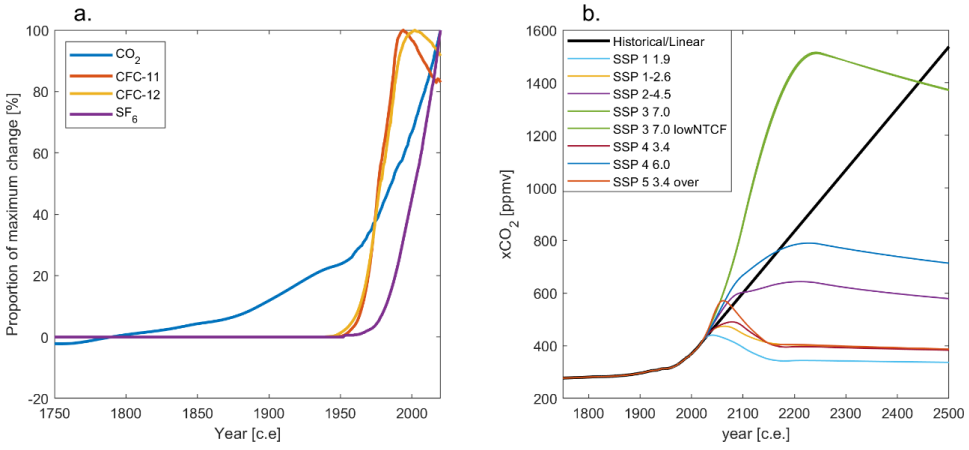

Figure 4. (a.) The time history of atmospheric transient tracer and CO_2 concentrations expressed as a percentage of their maximum deviation through 2020 c.e. from their assigned preindustrial values of 0 ppmv for CFC-11, CFC-12, and SF_6 and 280 ppmv for CO_2. **(b.)** The 9 atmospheric CO_2 concentration pathway options used by TRACEv1, with all but "Historical/Linear" being SSPs as given by Meinshausen et al. (2020). Both versions of SSP 3 7.0 fall nearly on top of each other on this plot and are assigned the same colors.

TRACEv1 allows 9+ options for atmospheric CO_2 projections/histories and relies on a single reconstruction of transient tracers (Fig. 4). Observed atmospheric CFC and SF_6 information (Fig. 4a) is taken from a data product compiled by the United States Geological Survey's Groundwater Dating Laboratory (see: data availability) The atmospheric xCO_2 reconstruction starting in the year 1 c.e. and continuing through the year 1000 is taken from the synthesis by Frank et al. (2010) for all CO_2 options. Before the year 1 c.e. all reconstructions are set to a constant value of xCO_2=277.14 ppmv equaling the atmospheric concentration in the year 1 c.e. From 1001 and through 1959, all reconstructions follow the historical concentrations of the SSPs as defined by Meinshausen et al. (2020), which are identical over this time range. From 1959 through 2022, the first option, which is called "Historical/Linear" and is the default option if no alternative is specified, uses the Mauna Loa measurements by Keeling et al. (1976) and Thoning et al. (1989), and if TRACEv1 is instructed to use this record to generate an estimate for a year that is after 2022 then the slope from a linear trend fit to the last 10 years of the historical record is used to project to the year of the desired estimate. The remaining 8 options are SSPs: 1_1.9, 1-2.6, 2-4.5, 3_7.0, 3_7.0_lowNTCF, 4_3.4, 4_6.0, and 5_3.4_over, all as defined by Meinshausen et al. (2020). The SSPs diverge from each other starting in 2017. Between year 1959 and 2017 c.e. the SSP values have a small average bias of +0.6 ppmv compared to the historical Mauna Loa measurements with a root-mean squared disagreement of 0.8 ppmv. Additional custom concentration pathways options can be added by appending a new column of atmospheric CO_2 concentrations to a plain text file (CO2trajectoriesAdjusted.txt) that is read by TRACEv1 and by entering the number of the new option in the TRACEv1 code (i.e., if a 10th option is added the CO_2 pathway option for the "AtmCO2Trajectory" input would be 10). However,

https://doi.org/10.5194/essd-2024-560
Preprint. Discussion started: 11 December 2024

it is recommended that any user provided concentration pathways be adjusted by equation 3 before appending them to this file.

3.4 Fitting TRACEv1 parameters

The parameters are optimized using a bounded minimum "search" function (fminsearchbnd in Matlab) with an initial value of α=1, an upper bound of α=1000, and a lower bound of α=0.001. For each iteration of this solver, the j=3 (i.e., CFC-11, CFC-12, and SF_6) transient tracer constraints and the A are first calculated as described in the previous section. The cost function that is minimized for this solver (ε^2) is the sum of the squared normalized errors of the three partial pressures and A, or:

$$\varepsilon^2 = \sum_{j=1}^{3}\left(\frac{pX^j_{\mathrm{meas}} - pX^j_{\mathrm{calc}}}{pX^j_{\mathrm{ATM\_2020}}}\right)^2 + \left(\frac{A_{\mathrm{OCIM}} - A_{\mathrm{calc}}}{A_{\mathrm{Max}}}\right)^2 \quad (4)$$

Here the pX^j_{meas} is the measured partial pressure of transient tracer j extracted from discrete GLODAPv2.2023 product or (for the model validation experiments) from GOBM output; pX^j_{calc} is the value calculated from α and the record of atmospheric trace gas concentrations as described above; and $pX^j_{\mathrm{ATM_2020}}$is the atmospheric partial pressure of tracer j in the year 2020. This third term is included to normalize the errors to a more comparable scale. Without this term, the pCFC-12 (SF_6) errors would be assigned higher (lower) weight than the errors in the other two transient tracers due to their greater (smaller) atmospheric partial pressures. Similarly, A_{OCIM} is the interpolated OCIM age, A_{calc} is the calculated A, and A_{max} is the ideal age of the oldest grid cell found in the OCIM age calculations (1354 years).

This process is repeated for the observational record and for the model output. The version of TRACEv1 that is trained on model output is referred to as TRACEv1_validation_NorESM, and details for this comparison are provided in Supplementary Text S6. The version trained on real world observations is referred to as TRACEv1. We generate 10 versions of TRACEv1 in which we retrain TRACEv1 after perturbing the transient tracer measurements from each cruise in GLODAPv2.2023 by a cruise-wide relative offset and each measurement by measurement-specific random perturbations. In Supplementary Text S7 we quantify the likely impact of measurement uncertainties in the transient tracer measurements on the final C_{anth} estimates via Monte Carlo analysis.

3.5 C_{anth} data product creation

We use the gridded, temporally-averaged GLODAPv2 data product Lauvset et al. (2016) for S, T, latitude, longitude, and depth and vary only the year of the estimate to equal [1750; 1800; 1850; 1900; 1950; 1980; 1994.5; 2000; 2002; 2007.5; 2010; 2014.5; 2020; 2030; 2050; and 2100]. Estimates are only made using the historical/linear and SSP1_1.9 reconstructions prior to 2010 (and we note that the SSPs are identical over this period). In 2020 and thereafter, estimates are provided for each of the 9 CO_2 concentration pathway options separately. The estimates in 1994.5, 2002, 2007, and 2014 are provided for comparison and interoperability with published literature distributions (Gruber et al., 2019a; Lauvset et al., 2016; Müller et al., 2023; Sabine et al., 2004).

https://doi.org/10.5194/essd-2024-560
Preprint. Discussion started: 11 December 2024

We anticipate that the small differences between the 1850 and 1750 CO_2 concentration estimates could prove useful for reconciling literature estimates of C_{anth} that have been made to be specific to these two common choices of reference year. Our C_{anth} definition is specific to the 280 ppmv atmospheric concentration rather than to a specific year. It is therefore possible for TRACEv1 to return very small negative C_{anth} values, particularly for estimates following periods when CO_2 reached minima of ~277±1 ppmv in the first, sixth, and eighteenth centuries c.e. The last time the atmospheric CO_2 concentration was believed to equal 280 ppmv was 1790 c.e. (Frank et al. 2010) and TRACEv1 allows users to specify an alternative reference concentration.

4 Results and discussion

We discuss the uncertainty assessment and compare TRACEv1 reconstructions to alternatives, discuss the TRACEv1 projections through 2500, and highlight some areas where TRACEv1 is limited and might be improved. We compare TRACEv1 A estimates to alternatives in Supplementary Text S8.

4.1 Uncertainty estimation

In Supplementary Text S5 we describe the results of our uncertainty assessments from model reconstruction ($_{MR}$) C_{anth} distributions. In Supplementary Text S6 we present the results of the Monte Carlo ($_{MC}$) analysis. Here, we combine the results of the analyses to estimate the uncertainty of TRACEv1 (U_{TRACEv1}) estimates that results from several sources. The model C_{anth} reconstruction estimates reveal methodological uncertainties including the limitations of an IG TTD and the inaccuracies associated with using a neural network across a large geographical area, as well as the uncertainties that result from potential OCIM A distribution and preformed property distribution errors. The Monte Carlo analysis reveals uncertainties that result from random uncertainties and cruise-wide offsets in transient tracer concentration measurements. We add these uncertainties in quadrature to obtain the overall uncertainty estimate (±1σ) for TRACEv1 (U_{TRACEv1}):

$$U_{\mathrm{TRACEv1}} = \sqrt{u_{\mathrm{MC}}^2 + u_{\mathrm{MR}}^2} \qquad (5)$$

Here, u_{MC} is the Monte Carlo RMSE estimate of 2 µmol kg^{-1} for C_{anth} and ±1.5 % for inventories, u_{MR} is the uncertainty estimate from the model reconstruction of 4.4 µmol kg^{-1} for C_{anth} and 15 % for inventories, since the model reconstruction reproduces inventories to within 12 % in 1980 and 2014. The uncertainty appears to grow with the estimate and over time, so 15 % of the estimated C_{anth} is used when this value exceeds 4.4 µmol kg^{-1}. These uncertainty estimates neglect the contribution of uncertainty in the S and T values used in the neural network to the overall C_{anth} estimate uncertainty, which we believe to be small relative to U_{TRACEv1}, but we note that users can conduct perturbation tests if they are supplying particularly uncertain S and T information. U_{TRACEv1} is an optional output from TRACEv1. In Supplementary Text S6 we show that reconstruction errors are significantly larger in marginal seas with few or no transient tracer measurements and are also elevated near coasts and in areas of strong upwelling. U_{TRACEv1} should be considered an underestimate in these regions. We do not attempt to estimate uncertainty in the optional A TRACEv1 output.

https://doi.org/10.5194/essd-2024-560
Preprint. Discussion started: 11 December 2024

380

4.2 C_{anth} reconstructions and data product comparisons

The reconstructions and projections from TRACEv1 (Table 1) match past anthropogenic inventory estimates obtained from analyses based on measurements of DIC changes and distributions (Fig. 5) in 1994 (118(±26) PgC from Sabine et al. (2004) vs. 121(±18) for TRACEv1), 2007 (118(±26)+29(±2.5)=147(±26) Pg C; Müller et al. (2023), updating
385 Gruber et al. 2019a vs. 156(±23) for TRACEv1), and 2014 (118(±26)+29(±2.5)+27(±2.5)=174(±26) Pg C from Müller et al. 2023 vs. 177(±26) for TRACEv1). The strong agreement with the DIC based approaches is reassuring, as there is little overlap in the data or methodologies used to generate the DIC-based estimates compared to the data and methods used to obtain the TRACEv1 routines: Müller et al. (2023), did not rely on transient tracer information and the CFC-11 and CFC-12 information used by Sabine et al. (2004) to quantify their disequilibrium term does not have
390 overlap with the information used in this study because these earlier measurements did not have collocated SF_6 content values (Fig. 1).

The regional distribution of C_{anth} inventory qualitatively matches prior estimates as well, with significantly higher column inventory estimates in the North Atlantic (Fig. 6; Table 1). Similarly, there are areas of higher column
395 inventories generally in the Southern Hemispheres of the other ocean basins as mode and intermediate waters are exported northward from the Southern Ocean. Within Figure 6, bathymetric features such as the Kerguelen Plateau and the Mid-Atlantic Ridge are visible when they displace waters that would otherwise contain meaningful quantities of C_{anth}, and a band of low column inventories can be seen within the Antarctic Circumpolar Current where old deep waters upwell to near the ocean surface.

400

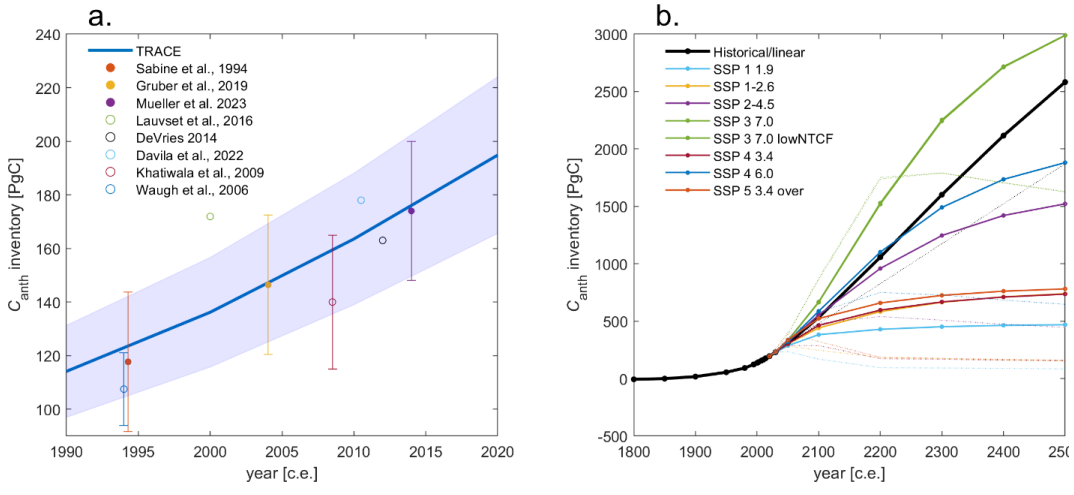

Figure 5. Panel **(a.)** shows the global C_{anth} inventory projected by TRACEv1 with a blue range indicating the uncertainty estimate. Circles show estimates from literature data-based C_{anth} distribution estimates with filled circles indicating estimates rooted primarily in DIC measurements and open circles indicating estimates rooted primarily in fitting transient tracer distributions. Panel **(b.)** shows projected values through 2500 c.e. in solid lines

https://doi.org/10.5194/essd-2024-560
Preprint. Discussion started: 11 December 2024

for various SSPs as labeled. Thin dotted lines indicate the inventories that would be obtained by projecting the 2020 c.e. estimate using transient steady state assumptions (Gammon et al., 1982) with the atmospheric CO_2 concentrations from the SSPs of the same color line. Both versions of SSP 3 7.0 fall nearly on top of each other on this plot and are assigned the same colors.

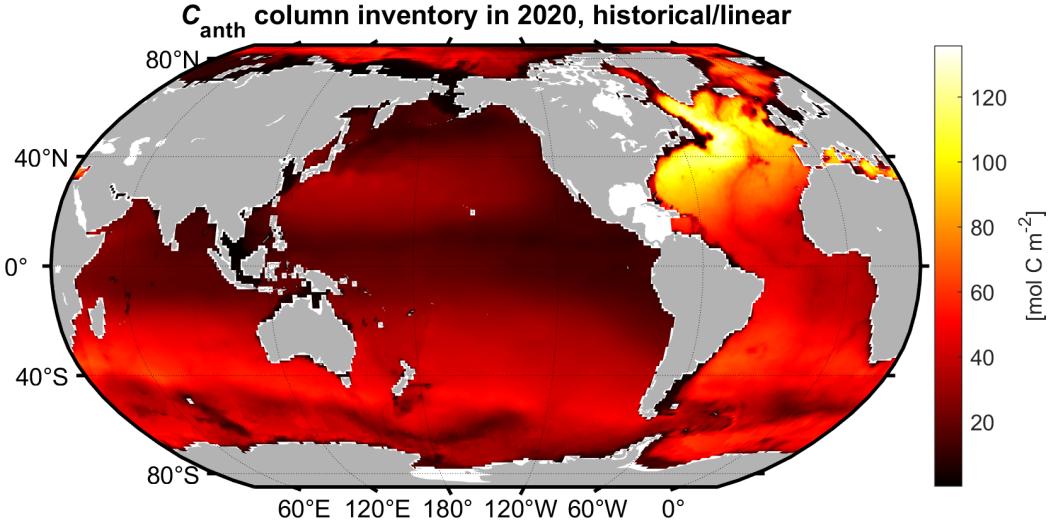

Figure 6. Column inventory of C_{anth} mapped for 2020 using TRACEv1 with the historical/linear atmospheric CO_2 pathway.

Table 1. TRACEv1 estimates of C_{anth} inventories (in PgC ±1σ uncertainties) calculated by ocean basin calculated for the specified points in time. The Atlantic becomes the Arctic at 40° N whereas the Pacific transitions at 67° N. The Southern Ocean is defined as the area in all basins south of 40° S. Anthropogenic inventories are small and negative in 1750 because of the ~200 year-long period with a <280 ppmv CO_2 atmosphere prior to the Industrial Era.

Year	Pacific	Atlantic	Indian	Arctic	Southern	Total
1750	-2(±1)	-2(±1)	-1(±1)	-1(±1)	-2(±1)	-8(±2)
1800	-1(±1)	-2(±1)	-1(±1)	0(±1)	-2(±1)	-6(±1)
1850	0(±1)	0(±1)	0(±1)	0(±1)	0(±1)	-1(±1)
1900	5(±1)	4(±1)	2(±1)	2(±1)	4(±1)	17(±3)
1950	14(±2)	14(±2)	7(±2)	6(±1)	13(±2)	55(±8)
1980	25(±4)	24(±4)	12(±2)	9(±2)	23(±4)	92(±14)
1994	34(±5)	31(±5)	16(±3)	11(±2)	30(±5)	123(±18)
2000	37(±6)	34(±5)	18(±3)	13(±2)	34(±5)	136(±20)
2002	39(±6)	36(±6)	19(±3)	13(±2)	35(±5)	143(±21)
2007	43(±7)	39(±6)	21(±3)	15(±2)	39(±6)	156(±23)
2010	45(±7)	41(±6)	22(±3)	15(±3)	40(±6)	164(±25)
2014	49(±7)	45(±7)	23(±4)	16(±3)	44(±7)	177(±27)
2020	54(±8)	49(±7)	26(±4)	18(±3)	48(±7)	195(±29)

https://doi.org/10.5194/essd-2024-560
Preprint. Discussion started: 11 December 2024

TRACEv1 has a more variable agreement with estimates based on transient tracer information. The estimates are slightly higher than—but within uncertainties of—the Green's function fits of Khatiwala et al. (2009) and a TTD based inventory estimate (Waugh et al., 2006). TRACEv1 estimates of 164(±24) PgC are within uncertainties of the 178 PgC inventory of Davila et al. (2022) calculated in 2010 using the Total Matrix Intercomparison approach. At 170 (±25) PgC, TRACEv1 estimates are near the OCIM estimates of Devries (2014) of 160-166 PgC in 2012, though this not surprising since the A estimates implied by an OCIM solution were used as a fitting parameter for TRACEv1. The TTD-based C_{anth} inventory for 2002 in the gridded GLODAPv2 data product of Lauvset et al. (2016) is 179 PgC compared to a TRACEv1 estimate of 143(±21) PgC in the same year. In Supplementary Text S9 we show that the main disagreement between the TRACE estimates and the GLODAPv2 gridded product (Lauvset et al., 2016) is found in the deep ocean, where GLODAPv2 inventories consistently exceed TRACE inventories below ~500 m. There are several possible reasons for this disagreement, but the true cause is unclear.

4.3 C_{anth} inventory projections

Table 2. TRACEv1 projections of global ocean C_{anth} inventories (in PgC) until the middle of the millennium if the indicated atmospheric CO_2 concentration pathway is followed.

	2020	2030	2050	2100	2200	2300	2400	2500
Historical/Linear	195(±29)	230(±34)	307(±46)	532(±80)	1057(±159)	1601(±240)	2116(±317)	2582(±387)
SSP_1_1.9	194(±29)	229(±34)	286(±43)	382(±57)	429(±64)	452(±68)	463(±70)	469(±70)
SSP_1_2.6	194(±29)	230(±35)	302(±45)	441(±66)	583(±87)	664(±100)	712(±107)	739(±111)
SSP_2_4.5	194(±29)	231(±35)	317(±48)	553(±83)	959(±144)	1246(±187)	1420(±213)	1522(±228)
SSP_3_7.0	194(±29)	233(±35)	332(±50)	668(±100)	1529(±229)	2253(±338)	2717(±408)	2991(±449)
SSP_3_7.0lowNTCF	194(±29)	233(±35)	331(±50)	664(±100)	1519(±228)	2244(±337)	2711(±407)	2988(±448)
SSP_4_3.4	194(±29)	230(±34)	303(±45)	463(±69)	596(±89)	667(±100)	710(±107)	736(±110)
SSP_4_6.0	194(±29)	231(±35)	320(±48)	587(±88)	1102(±165)	1491(±224)	1735(±260)	1881(±282)
SSP_5_3.4over	194(±29)	233(±35)	337(±50)	523(±78)	658(±99)	725(±109)	761(±114)	781(±117)

The C_{anth} inventory projections (Table 2, Fig. 5b) indicate that even if humanity acts to rapidly reduce C_{anth} in the atmosphere and manages to bring atmospheric xCO_2 down to 337 µatm by the middle of the millennium in line with the ambitious SSP 1_1.9, the ocean will never—on this time horizon—cease to take up additional C_{anth}, picking up an additional 5.6 PgC between 2400 and 2500 c.e. This builds on the findings of Koven et al. (2022) and Jones et al. (2016) using full model simulations through 2300 c.e., and suggests that the impacts of ocean acidification are likely to continue to spread throughout the ocean depths even with a highly successful carbon management policy. Nevertheless, such action remains important for preventing ocean acidification because the degree of surface and interior ocean acidification depends strongly on which SSP we follow. This is particularly true for the well-lit surface euphotic zone that is the base of most marine food webs: the relative proportion of marine C_{anth} shifts increasingly from the surface ocean to the ocean depths over time (Fig. 7a), and this tendency becomes more pronounced the more rapidly and completely that atmospheric CO_2 emissions are curtailed and reversed (Fig. 7b). Indeed, several SSPs show reduced surface C_{anth} relative to modern values despite the continued ocean C_{anth} accumulation. An important caveat is that these findings do not consider the impacts of changes in heat and freshwater content, circulation, or

https://doi.org/10.5194/essd-2024-560
Preprint. Discussion started: 11 December 2024

changes in the ocean's biological pump, and only reflect the impact expected from changing atmospheric xCO_2 and ocean buffer capacity.

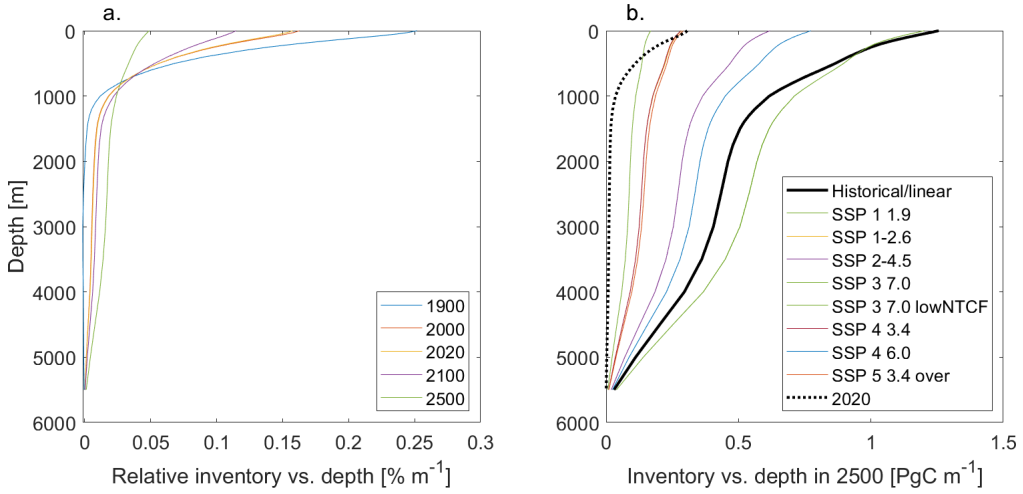

Figure 7. (a.) The relative inventory of C_{anth} vs. depth in various years of the historical/linear projection, expressed as the percentage of the total DIC inventory that is found within each 1 m interval. Here, a shrinking surface value indicates a greater proportion of the signal is found at depth, but does not necessarily imply a lesser surface C_{anth}. Panel **(b.)** shows the total inventory in 2500 vs. depth in solid lines for each of the CO_2 concentration pathways used by TRACEv1, with the 2020 historical/linear inventory plotted as a dashed line for comparison. Both versions of SSP 3 7.0 fall nearly on top of each other on this plot and are assigned the same colors.

One intended use for TRACEv1 is adjusting DIC measurement to a reference year. The simple approximation of transient steady state (Gammon et al., 1982) has been used in several recent studies (e.g., Lauvset et al. 2016; Clement and Gruber 2018; Carter et al. 2021a; Müller et al. 2023), and our projections show that this assumption performs plausibly for projections over short timescales. However, we contend that TRACEv1 provides a superior means of adjusting DIC measurements to be appropriate for a reference year. For example, the differences between modeled C_{anth} between 1980 and 2014 in NorESM disagree with the differences between TRACEv1 estimates for those same years by an average of −0.1 (±3.2) µmol kg^{-1}. The statistics are somewhat worse at −1.2 (±3.6) µmol kg^{-1} when same differences are compared instead to the differences between the 1980 C_{anth} values and the 1980 values scaled to 2014 using transient steady state assumptions. Thus, both adjustments are reasonable from 1980 to 2014, but the transient steady state adjustment tends to overpredict the change. Also, unlike TRACEv1, transient steady state adjustments require an independent estimate of C_{anth} (for the comparison above they were provided the exactly-correct model C_{anth} distribution in the earlier year, though this is never known in the real ocean) Finally, the transient steady state assumption is also known to break down if the atmosphere ceases to increase in its tracer concentration exponentially, and this occurs for CO_2 in all SSPs by 2500 c.e. and in most of them much sooner (Meinshausen et al., 2020). It can be seen in these cases that transient steady state results in large errors in the projected C_{anth} inventories by mid-millennium and even projects spurious decreases (Fig. 5b).

https://doi.org/10.5194/essd-2024-560
Preprint. Discussion started: 11 December 2024

4.4 Limitations and future directions

There are several notable limitations of the TRACEv1 method:

1. It presumes fixed circulation and is unable to resolve most timescales and modes of C_{anth} variability.
2. It also shows larger reconstruction errors in regions that lack training data, which is a common problem for neural networks and other regression strategies (e.g., Carter et al., 2021). As transient tracer measurements with the strong SF_6 constraint are still relatively rare (approximately 5 % of the GLODAPv2.2023 data product contains all three transient tracer measurements), it is likely that TRACE will improve as more such measurements become incorporated. However, version 1 of TRACE should be used with caution in regions without training data, and this caution applies to many marginal seas (Figs. 1 and S1).
3. TRACEv1 also appears to overestimate C_{anth} in surface waters where there is meaningful upwelling, though perhaps not by a larger extent than alternative C_{anth} estimation strategies. This is unfortunate because such surface waters are frequently found in areas of naturally low pH that are of interest for ocean acidification research.
4. The method also has not yet been well validated in a high-resolution model representation of a coastal environment, so its uncertainties are not well estimated outside of the open ocean. While the circulation information encoded in TRACEv1 has been optimized within a limited parameter space, it is likely—based on past literature exploring many options for simplifying the complex distributions of myriad water types that mix in the ocean interior—that the comparatively simple single term that we employ herein to constrain interior ocean age distributions could be meaningfully improved. We leave this to future work.
5. Furthermore, the TTD approach is limited by the need for an assumed air-sea disequilibrium and the possibility that the degree of disequilibrium for transient tracers varies meaningfully over time and between CFCs and SF_6 (Shao et al., 2013; Sonnerup et al., 2015) and differs from the related term for air-sea CO_2 disequilibria, which seems likely due to the slow relaxation of CO_2 disequilibria (Jones et al., 2014) and the faster rate of transient tracer equilibration (Wanninkhof 2014). A common assumption of 100 % equilibration tends to result in TTD approaches overestimating the C_{anth} (Waugh et al., 2006). We include an empirical relationship intended to deal with this issue but note that its formulation remains somewhat ad hoc and based on model simulations of surface ocean conditions.
6. TRACEv1 is aimed at resolving the accumulation of C_{anth} under "steady state" circulation. However, it is possible that it is able to resolve some non-steady-state components of C_{anth} accumulation when it is called with time-varying temperature and salinity records as predictors. It is yet untested to what degree this is an effective strategy for capturing such variability.

We include the version number in TRACEv1 both to signal that future improvements are likely and to disambiguate the function from other software routines that might have similar names. There are several ways that TRACEv1 might be improved.

https://doi.org/10.5194/essd-2024-560
Preprint. Discussion started: 11 December 2024

1. Some fitting strategies have shown improvements when the signal of interest is fit to the disagreement between observations and a model prior, instead of being fit directly to the signal. This approach could improve estimates if a model prior age distribution can be obtained and be re-gridded to global locations of interest in a computationally efficient manner.
2. Further optimization of the shape of the TTD could result in improved C_{anth} reconstructions.
3. MATLAB is an open-source language, but it is not freely available. It would therefore further improve the accessibility of C_{anth} estimates if TRACEv1 were released in a freely-available computing package. Prior experience suggests that a modest amount of script is required to convert neural-networks from Matlab to Python, and somewhat less is required to transition the code to Julia. This is left to future work.

5 Data availability statement

The gridded GLODAP product is available at https://glodap.info/. The CFC and SF_6 atmospheric record data product was obtained from the USGS Groundwater Dating Lab website https://water.usgs.gov/lab/software/air_curve/index.html. The TRACEv1_GGC_{anth} product is available at Zenodo https://doi.org/10.5281/zenodo.14003665 (Carter, 2024).

6 Code availability statement

TRACEv1 code can be found and freely obtained at https://github.com/BRCScienceProducts/TRACEv1.

7 Conclusions

We present a new method called TRACEv1 for rapidly estimating the time varying C_{anth} distribution throughout the open ocean, including detailed error estimates. TRACEv1 is available as a function in the MATLAB programming language. We further provide a data product with C_{anth} distributions for a range of years (TRACEv1_GGC_{anth}, Carter, 2024) on the GLODAPv2 gridded product grid used by Lauvset et al. (2016). We use this data product to examine how the C_{anth} distribution varies with depth and time and show that the ocean can be expected to continue to increase its C_{anth} inventory through 2500 c.e. for all SSPs. We find that SSP_3_7.0 results in the largest projected 2500 ocean C_{anth} inventory of 2991 (±449) PgC, and this represents a ~15-fold increase over the 2020 C_{anth} inventory.

There are several strengths of the TRACEv1 method, which relies on TTDs to estimate C_{anth} distributions from a time-evolving atmospheric CO_2 trajectory. The method is easy and quick to implement, shows fidelity to model reconstructions and agreement with recently published data-based estimates, and only requires S and T measurements and spatiotemporal coordinate information to produce an estimate. It also provides means to plausibly adjust collections of DIC measurements collected over time to a common time by removing the influences of C_{anth} changes. While the reconstruction fidelity of TRACEv1 estimates were quite high in a test using model output with exactly known C_{anth} distributions, we nevertheless believe the primary advantages of TRACEv1 and the new data product are their accessibility.

https://doi.org/10.5194/essd-2024-560
Preprint. Discussion started: 11 December 2024

8 Competing interests

The authors declare they have no conflict of interest.

9 Acknowledgements

We thank the PIs and analysts who have spent decades laboring to collect the transient tracer information that makes TRACEv1 and the data product possible. BRC thanks US National Science Foundation for the funds to develop TRACEv1 under "Collaborative Research: Improving the accuracy and uncertainty associated with estimated pCO_2 from pH sensors on autonomous profiling platforms" (award number 2048509, program officer: Henrietta Edmonds). The data synthesis efforts, comparisons to alternative estimates, and development of the preformed property neural networks were performed with the support of the Global Ocean Monitoring and Observing program of NOAA through funding the Carbon Data Management and Synthesis Program (Fund Ref. 100007298, program officer: Kathy Tedesco). LMD's contributions are made with support from the Biogeochemical Argo Algorithms grant from NOAA's Climate Variability and Global Ocean and Monitoring Observation Programs (award number NA21OAR4310251, program officer: Virginia Selz). The PMEL and CICOES contributions are numbers 5695 and 2024-1424, respectively. AJF's contribution was supported by PMEL, RES's by NSF award 1634256, JDS's by PMEL and the Cooperative Institute for Climate, Ocean, and Ecosystem Studies (CICOES) under Cooperative Agreement NA20OAR4320271.

10 References

Bolin, B. and Rodhe, H.: A note on the concepts of age distribution and transit time in natural reservoirs, Tellus, 25, 58–62, https://doi.org/10.1111/j.2153-3490.1973.tb01594.x, 1973.

Bullister, J. L., Wisegarver, D. P., and Menzia, F. A.: The solubility of sulfur hexafluoride in water and seawater, Deep Sea Res. Part Oceanogr. Res. Pap., 49, 175–187, https://doi.org/10.1016/S0967-0637(01)00051-6, 2002.

Bullister, J. L., Wisegarver, D. P., and Sonnerup, R. E.: Sulfur hexafluoride as a transient tracer in the North Pacific Ocean, Geophys. Res. Lett., 33, https://doi.org/10.1029/2006GL026514, 2006.

Carter, B. R.: Anthropogenic carbon distributions from preindustrial to 2500 c.e. estimated using Tracer-based Rapid Anthropogenic Carbon Estimation (version 1) (Pre-submission for peer-review), https://doi.org/10.5281/zenodo.14003665, 2024.

Carter, B. R., Feely, R. A., Wanninkhof, R., Kouketsu, S., Sonnerup, R. E., Pardo, P. C., Sabine, C. L., Johnson, G. C., Sloyan, B. M., Murata, A., Mecking, S., Tilbrook, B., Speer, K., Talley, L. D., Millero, F. J., Wijffels, S. E., Macdonald, A. M., Gruber, N., and Bullister, J. L.: Pacific Anthropogenic Carbon Between 1991 and 2017, Glob. Biogeochem. Cycles, 2018GB006154, https://doi.org/10.1029/2018GB006154, 2019.

Carter, B. R., Bittig, H. C., Fassbender, A. J., Sharp, J. D., Takeshita, Y., Xu, Y. Y., Álvarez, M., Wanninkhof, R., Feely, R. A., and Barbero, L.: New and updated global empirical seawater property estimation routines, Limnol. Oceanogr. Methods, https://doi.org/10.1002/LOM3.10461, 2021a.

https://doi.org/10.5194/essd-2024-560
Preprint. Discussion started: 11 December 2024

Carter, B. R., Feely, R. A., Lauvset, S. K., Olsen, A., DeVries, T., and Sonnerup, R.: Preformed Properties for Marine Organic Matter and Carbonate Mineral Cycling Quantification, Glob. Biogeochem. Cycles, 35, e2020GB006623, https://doi.org/10.1029/2020GB006623, 2021b.

Clement, D. and Gruber, N.: The eMLR(C*) method to determine decadal changes in the global ocean storage of anthropogenic CO_2, Glob. Biogeochem. Cycles, https://doi.org/10.1002/2017GB005819, 2018.

Davila, X., Gebbie, G., Brakstad, A., Lauvset, S. K., McDonagh, E. L., Schwinger, J., and Olsen, A.: How Is the Ocean Anthropogenic Carbon Reservoir Filled?, Glob. Biogeochem. Cycles, 36, e2021GB007055, https://doi.org/10.1029/2021GB007055, 2022.

Devries, T.: The oceanic anthropogenic CO_2 sink: Storage, air-sea fluxes, and transports over the industrial era, Glob. Biogeochem. Cycles, 28, 631–647, https://doi.org/10.1002/2013GB004739, 2014.

DeVries, T., Holzer, M., and Primeau, F.: Recent increase in oceanic carbon uptake driven by weaker upper-ocean overturning, Nature, 542, 215–218, https://doi.org/10.1038/nature21068, 2017.

DeVries, T., Yamamoto, K., Wanninkhof, R., Gruber, N., Hauck, J., Müller, J. D., Bopp, L., Carroll, D., Carter, B., Chau, T.-T.-T., Doney, S. C., Gehlen, M., Gloege, L., Gregor, L., Henson, S., Kim, J. H., Iida, Y., Ilyina, T., Landschützer, P., Le Quéré, C., Munro, D., Nissen, C., Patara, L., Pérez, F. F., Resplandy, L., Rodgers, K. B., Schwinger, J., Séférian, R., Sicardi, V., Terhaar, J., Triñanes, J., Tsujino, H., Watson, A., Yasunaka, S., and Zeng, J.: Magnitude, Trends, and Variability of the Global Ocean Carbon Sink From 1985 to 2018, Glob. Biogeochem. Cycles, 37, e2023GB007780, https://doi.org/10.1029/2023GB007780, 2023.

Dickson, A. G. (Andrew G., Sabine, C. L., Christian, J. R., and North Pacific Marine Science Organization.: Guide to best practices for ocean CO_2 measurements, North Pacific Marine Science Organization, 2007.

Doney, S. C., Fabry, V. J., Feely, R. A., and Kleypas, J. A.: Ocean acidification: the other CO_2 problem., Annu. Rev. Mar. Sci., 1, 169–192, https://doi.org/10.1146/annurev.marine.010908.163834, 2009.

Doney, S. C., Busch, D. S., Cooley, S. R., and Kroeker, K. J.: The impacts of ocean acidification on marine ecosystems and reliant human communities, Annu. Rev. Environ. Resour., 45, 83–112, https://doi.org/10.1146/annurev-environ-012320-083019, 2020.

Eide, M., Olsen, A., Ninnemann, U. S., and Eldevik, T.: A global estimate of the full oceanic 13C Suess effect since the preindustrial, Glob. Biogeochem. Cycles, 31, 492–514, https://doi.org/10.1002/2016GB005472, 2017.

Erickson, Z. K., Carter, B. R., Feely, R. A., Johnson, G. C., Sharp, J. D., and Sonnerup, R. E.: Pmel's Contribution to Observing and Analyzing Decadal Global Ocean Changes Through Sustained Repeat Hydrography, Oceanography, 36, 60–69, 2023.

Frank, D. C., Esper, J., Raible, C. C., Büntgen, U., Trouet, V., Stocker, B., and Joos, F.: Ensemble reconstruction constraints on the global carbon cycle sensitivity to climate, Nature, 463, 527–530, https://doi.org/10.1038/nature08769, 2010.

Friedlingstein, P., O'Sullivan, M., Jones, M. W., Andrew, R. M., Gregor, L., Hauck, J., Le Quéré, C., Luijkx, I. T., Olsen, A., Peters, G. P., Peters, W., Pongratz, J., Schwingshackl, C., Sitch, S., Canadell, J. G., Ciais, P., Jackson, R. B., Alin, S. R., Alkama, R., Arneth, A., Arora, V. K., Bates, N. R., Becker, M.,

https://doi.org/10.5194/essd-2024-560
Preprint. Discussion started: 11 December 2024

Bellouin, N., Bittig, H. C., Bopp, L., Chevallier, F., Chini, L. P., Cronin, M., Evans, W., Falk, S., Feely, R. A., Gasser, T., Gehlen, M., Gkritzalis, T., Gloege, L., Grassi, G., Gruber, N., Gürses, Ö., Harris, I., Hefner, M., Houghton, R. A., Hurtt, G. C., Iida, Y., Ilyina, T., Jain, A. K., Jersild, A., Kadono, K., Kato, E., Kennedy, D., Klein Goldewijk, K., Knauer, J., Korsbakken, J. I., Landschützer, P., Lefèvre, N., Lindsay, K., Liu, J., Liu, Z., Marland, G., Mayot, N., McGrath, M. J., Metzl, N., Monacci, N. M., Munro, D. R., Nakaoka, S.-I., Niwa, Y., O'Brien, K., Ono, T., Palmer, P. I., Pan, N., Pierrot, D., Pocock, K., Poulter, B., Resplandy, L., Robertson, E., Rödenbeck, C., Rodriguez, C., Rosan, T. M., Schwinger, J., Séférian, R., Shutler, J. D., Skjelvan, I., Steinhoff, T., Sun, Q., Sutton, A. J., Sweeney, C., Takao, S., Tanhua, T., Tans, P. P., Tian, X., Tian, H., Tilbrook, B., Tsujino, H., Tubiello, F., van der Werf, G. R., Walker, A. P., Wanninkhof, R., Whitehead, C., Willstrand Wranne, A., et al.: Global Carbon Budget 2022, Earth Syst. Sci. Data, 14, 4811–4900, https://doi.org/10.5194/ESSD-14-4811-2022, 2022.

Gammon, R. H., Cline, J., and Wisegarver, D.: Chlorofluoromethanes in the northeast Pacific Ocean: Measured vertical distributions and application as transient tracers of upper ocean mixing, J. Geophys. Res., 87, 9441, https://doi.org/10.1029/JC087iC12p09441, 1982.

Gruber, N., Clement, D., Carter, B. R., Feely, R. A., Heuven, S. van, Hoppema, M., Ishii, M., Key, R. M., Kozyr, A., Lauvset, S. K., Monaco, C. L., Mathis, J. T., Murata, A., Olsen, A., Perez, F. F., Sabine, C. L., Tanhua, T., and Wanninkhof, R.: The oceanic sink for anthropogenic CO_2 from 1994 to 2007, Science, 363, 1193–1199, https://doi.org/10.1126/SCIENCE.AAU5153, 2019a.

Gruber, N., Landschützer, P., and Lovenduski, N. S.: The Variable Southern Ocean Carbon Sink, Annu. Rev. Mar. Sci., 11, 16.1-16.28, https://doi.org/10.1146/annurev-marine-121916-063407, 2019b.

Hall, T. M. and Haine, T. W. N.: On Ocean Transport Diagnostics: The Idealized Age Tracer and the Age Spectrum, J. Phys. Oceanogr., 32, 1987–1991, https://doi.org/10.1175/1520-0485(2002)032<1987:OOTDTI>2.0.CO;2, 2002.

Hall, T. M., Haine, T. W. N., and Waugh, D. W.: Inferring the concentration of anthropogenic carbon in the ocean from tracers, Glob. Biogeochem. Cycles, 16, 78-1-78–15, https://doi.org/10.1029/2001GB001835, 2002.

He, Y.-C., Tjiputra, J., Langehaug, H. R., Jeansson, E., Gao, Y., Schwinger, J., and Olsen, A.: A Model-Based Evaluation of the Inverse Gaussian Transit-Time Distribution Method for Inferring Anthropogenic Carbon Storage in the Ocean, J. Geophys. Res. Oceans, 123, 1777–1800, https://doi.org/10.1002/2017JC013504, 2018.

Ito, T. and Wang, O.: Transit Time Distribution based on the ECCO-JPL Ocean Data Assimilation, J. Mar. Syst., 167, 1–10, https://doi.org/10.1016/j.jmarsys.2016.10.015, 2017.

Jiang, L.-Q., Dunne, J., Carter, B. R., Tjiputra, J. F., Terhaar, J., Sharp, J. D., Olsen, A., Alin, S., Bakker, D. C. E., Feely, R. A., Gattuso, J.-P., Hogan, P., Ilyina, T., Lange, N., Lauvset, S. K., Lewis, E. R., Lovato, T., Palmieri, J., Santana-Falcón, Y., Schwinger, J., Séférian, R., Strand, G., Swart, N., Tanhua, T., Tsujino, H., Wanninkhof, R., Watanabe, M., Yamamoto, A., and Ziehn, T.: Global Surface Ocean Acidification Indicators From 1750 to 2100, J. Adv. Model. Earth Syst., 15, e2022MS003563, https://doi.org/10.1029/2022MS003563, 2023.

John, S. G., Liang, H., Weber, T., DeVries, T., Primeau, F., Moore, K., Holzer, M., Mahowald, N., Gardner, W., Mishonov, A., Richardson, M. J., Faugere, Y., and Taburet, G.: AWESOME OCIM: A simple, flexible, and powerful tool for modeling elemental cycling in the oceans, Chem. Geol., 533, 119403, https://doi.org/10.1016/j.chemgeo.2019.119403, 2020.

https://doi.org/10.5194/essd-2024-560
Preprint. Discussion started: 11 December 2024

Jones, C. D., Ciais, P., Davis, S. J., Friedlingstein, P., Gasser, T., Peters, G. P., Rogelj, J., Vuuren, D. P. van, Canadell, J. G., Cowie, A., Jackson, R. B., Jonas, M., Kriegler, E., Littleton, E., Lowe, J. A., Milne, J., Shrestha, G., Smith, P., Torvanger, A., and Wiltshire, A.: Simulating the Earth system response to negative emissions, Environ. Res. Lett., 11, 095012, https://doi.org/10.1088/1748-9326/11/9/095012, 2016.

Jones, D. C., Ito, T., Takano, Y., and Hsu, W.-C.: Spatial and seasonal variability of the air-sea equilibration timescale of carbon dioxide, Glob. Biogeochem. Cycles, 28, 1163–1178, https://doi.org/10.1002/2014GB004813, 2014.

Keeling, C. D., Bacastow, R. B., Bainbridge, A. E., Ekdahl Jr., C. A., Guenther, P. R., Waterman, L. S., and Chin, J. F. S.: Atmospheric carbon dioxide variations at Mauna Loa Observatory, Hawaii, Tellus, 28, 538–551, https://doi.org/10.3402/tellusa.v28i6.11322, 1976.

Khatiwala, S., Primeau, F., and Hall, T.: Reconstruction of the history of anthropogenic CO_2 concentrations in the ocean., Nature, 462, 346–9, https://doi.org/10.1038/nature08526, 2009.

Khatiwala, S., Tanhua, T., Mikaloff Fletcher, S., Gerber, M., Doney, S. C., Graven, H. D., Gruber, N., McKinley, G. A., Murata, A., Ríos, A. F., and Sabine, C. L.: Global ocean storage of anthropogenic carbon, Biogeosciences, 10, 2169–2191, https://doi.org/10.5194/bg-10-2169-2013, 2013.

Koven, C. D., Arora, V. K., Cadule, P., Fisher, R. A., Jones, C. D., Lawrence, D. M., Lewis, J., Lindsay, K., Mathesius, S., Meinshausen, M., Mills, M., Nicholls, Z., Sanderson, B. M., Séférian, R., Swart, N. C., Wieder, W. R., and Zickfeld, K.: Multi-century dynamics of the climate and carbon cycle under both high and net negative emissions scenarios, Earth Syst. Dyn., 13, 885–909, https://doi.org/10.5194/esd-13-885-2022, 2022.

Lauvset, S. K., Key, R. M., Olsen, A., Heuven, S. van, Velo, A., Lin, X., Schirnick, C., Kozyr, A., Tanhua, T., Hoppema, M., Jutterström, S., Steinfeldt, R., Jeansson, E., Ishii, M., Perez, F. F., Suzuki, T., and Watelet, S.: A new global interior ocean mapped climatology: the 1° × 1° GLODAP version 2, Earth Syst. Sci. Data, 8, 325–340, https://doi.org/10.5194/ESSD-8-325-2016, 2016.

Lauvset, S. K., Lange, N., Tanhua, T., Bittig, H. C., Olsen, A., Kozyr, A., Alin, S., Álvarez, M., Azetsu-Scott, K., Barbero, L., Becker, S., Brown, P. J., Carter, B. R., da Cunha, L. C., Feely, R. A., Hoppema, M., Humphreys, M. P., Ishii, M., Jeansson, E., Jiang, L.-Q., Jones, S. D., Lo Monaco, C., Murata, A., Müller, J. D., Pérez, F. F., Pfeil, B., Schirnick, C., Steinfeldt, R., Suzuki, T., Tilbrook, B., Ulfsbo, A., Velo, A., Woosley, R. J., and Key, R. M.: GLODAPv2.2022: the latest version of the global interior ocean biogeochemical data product, Earth Syst. Sci. Data, 14, 5543–5572, https://doi.org/10.5194/ESSD-14-5543-2022, 2022.

Lauvset, S. K., Lange, N., Tanhua, T., Bittig, H. C., Olsen, A., Kozyr, A., Álvarez, M., Azetsu-Scott, K., Brown, P. J., Carter, B. R., Cotrim da Cunha, L., Hoppema, M., Humphreys, M. P., Ishii, M., Jeansson, E., Murata, A., Müller, J. D., Perez, F. F., Schirnick, C., Steinfeldt, R., Suzuki, T., Ulfsbo, A., Velo, A., Woosley, R. J., and Key, R.: The annual update GLODAPv2.2023: the global interior ocean biogeochemical data product, Earth Syst. Sci. Data Discuss., 1–32, https://doi.org/10.5194/essd-2023-468, 2024.

Lueker, T. J., Dickson, A. G., and Keeling, C. D.: Ocean pCO2 calculated from dissolved inorganic carbon, alkalinity, and equations for K1 and K2: validation based on laboratory measurements of CO2 in gas and seawater at equilibrium, Mar. Chem., 70, 105–119, https://doi.org/10.1016/S0304-4203(00)00022-0, 2000.

https://doi.org/10.5194/essd-2024-560
Preprint. Discussion started: 11 December 2024

Matsumoto, K. and Gruber, N.: How accurate is the estimation of anthropogenic carbon in the ocean? An evaluation of the ΔC* method, Glob. Biogeochem. Cycles, 19, https://doi.org/10.1029/2004GB002397, 2005.

Meinshausen, M., Nicholls, Z. R. J., Lewis, J., Gidden, M. J., Vogel, E., Freund, M., Beyerle, U., Gessner, C., Nauels, A., Bauer, N., Canadell, J. G., Daniel, J. S., John, A., Krummel, P. B., Luderer, G., Meinshausen, N., Montzka, S. A., Rayner, P. J., Reimann, S., Smith, S. J., van den Berg, M., Velders, G. J. M., Vollmer, M. K., and Wang, R. H. J.: The shared socio-economic pathway (SSP) greenhouse gas concentrations and their extensions to 2500, Geosci. Model Dev., 13, 3571–3605, https://doi.org/10.5194/gmd-13-3571-2020, 2020.

Müller, J. D.: RECCAP2-ocean data collection, https://doi.org/10.5281/zenodo.7990823, 2023.

Müller, J. D., Gruber, N., Carter, B., Feely, R., Ishii, M., Lange, N., Lauvset, S. K., Murata, A., Olsen, A., Pérez, F. F., Sabine, C., Tanhua, T., Wanninkhof, R., and Zhu, D.: Decadal Trends in the Oceanic Storage of Anthropogenic Carbon From 1994 to 2014, AGU Adv., 4, e2023AV000875, https://doi.org/10.1029/2023AV000875, 2023.

Naveira Garabato, A. C., Jullion, L., Stevens, D. P., Heywood, K. J., and King, B. A.: Variability of Subantarctic Mode Water and Antarctic Intermediate Water in the Drake Passage during the Late-Twentieth and Early-Twenty-First Centuries, J. Clim., 22, 3661–3688, https://doi.org/10.1175/2009JCLI2621.1, 2009.

Peacock, S. and Maltrud, M.: Transit-Time Distributions in a Global Ocean Model, https://doi.org/10.1175/JPO2860.1, 2006.

Perez, F. F. and Fraga, F.: Association constant of fluoride and hydrogen ions in seawater, Mar. Chem., 21, 161–168, https://doi.org/10.1016/0304-4203(87)90036-3, 1987.

Sabine, C. L., Feely, R. A., Gruber, N., Key, R. M., Lee, K., Bullister, J. L., Wanninkhof, R., Wong, C. S., Wallace, D. W. R., Tilbrook, B., Millero, F. J., Peng, T.-H., Kozyr, A., Ono, T., and Rios, A. F.: The oceanic sink for anthropogenic CO_2., Science, 305, 367–71, https://doi.org/10.1126/science.1097403, 2004.

Shao, A. E., Mecking, S., Thompson, L., and Sonnerup, R. E.: Mixed layer saturations of CFC-11, CFC-12, and SF6 in a global isopycnal model, J. Geophys. Res. Oceans, 118, 4978–4988, https://doi.org/10.1002/jgrc.20370, 2013.

Sonnerup, R. E., Mecking, S., and Bullister, J. L.: Transit time distributions and oxygen utilization rates in the Northeast Pacific Ocean from chlorofluorocarbons and sulfur hexafluoride, Deep Sea Res. Part Oceanogr. Res. Pap., 72, 61–71, https://doi.org/10.1016/j.dsr.2012.10.013, 2013.

Sonnerup, R. E., Mecking, S., Bullister, J. L., and Warner, M. J.: Transit time distributions and oxygen utilization rates from chlorofluorocarbons and sulfur hexafluoride in the Southeast Pacific Ocean, J. Geophys. Res. Oceans, 120, 3761–3776, https://doi.org/10.1002/2015JC010781, 2015.

Stanley, R. H. R., Doney, S. C., Jenkins, W. J., and Lott, I. I. I.: Apparent oxygen utilization rates calculated from tritium and helium-3 profiles at the Bermuda Atlantic Time-series Study site, Biogeosciences, 9, 1969–1983, https://doi.org/10.5194/bg-9-1969-2012, 2012.

https://doi.org/10.5194/essd-2024-560
Preprint. Discussion started: 11 December 2024

Tanhua, T., Anders Olsson, K., and Fogelqvist, E.: A first study of SF6 as a transient tracer in the Southern Ocean, Deep Sea Res. Part II Top. Stud. Oceanogr., 51, 2683–2699, https://doi.org/10.1016/j.dsr2.2001.02.001, 2004.

Thiele, G. and Sarmiento, J. L.: Tracer dating and ocean ventilation, J. Geophys. Res. Oceans, 95, 9377–9391, https://doi.org/10.1029/JC095iC06p09377, 1990.

Thoning, K. W., Tans, P. P., and Komhyr, W. D.: Atmospheric carbon dioxide at Mauna Loa Observatory: 2. Analysis of the NOAA GMCC data, 1974–1985, J. Geophys. Res. Atmospheres, 94, 8549–8565, https://doi.org/10.1029/JD094iD06p08549, 1989.

Touratier, F. and Goyet, C.: Applying the new TrOCA approach to assess the distribution of anthropogenic CO2 in the Atlantic Ocean, J. Mar. Syst., 46, 181–197, https://doi.org/10.1016/j.jmarsys.2003.11.020, 2004.

Uppström, L. R.: The boron/chlorinity ratio of deep-sea water from the Pacific Ocean, Deep Sea Res. Oceanogr. Abstr., 21, 161–162, https://doi.org/10.1016/0011-7471(74)90074-6, 1974.

Van Heuven, S., Pierrot, D., Rae, J. W. B., Lewis, E., and Wallace, D. W. R.: MATLAB program developed for CO_2 system calculations, CO2sys., Carbon Dioxide Information Analysis Center, Oak Ridge National Laboratory, Oak Ridge, TN, 2011.

Vázquez-Rodríguez, M., Touratier, F., Lo Monaco, C., Waugh, D. W., Padin, X. A., Bellerby, R. G. J., Goyet, C., Metzl, N., Ríos, A. F., and Pérez, F. F.: Anthropogenic carbon distributions in the Atlantic Ocean: data-based estimates from the Arctic to the Antarctic, Biogeosciences, 6, 439–451, https://doi.org/10.5194/bg-6-439-2009, 2009.

Warner, M. J. and Weiss, R. F.: Solubilities of chlorofluorocarbons 11 and 12 in water and seawater, Deep Sea Res. Part Oceanogr. Res. Pap., 32, 1485–1497, https://doi.org/10.1016/0198-0149(85)90099-8, 1985.

Waugh, D. W., Hall, T. M., and Haine, T. W. N.: Relationships among tracer ages, J. Geophys. Res. Oceans, 108, https://doi.org/10.1029/2002JC001325, 2003.

Waugh, D. W., Haine, T. W. N., and Hall, T. M.: Transport times and anthropogenic carbon in the subpolar North Atlantic Ocean, Deep Sea Res. Part Oceanogr. Res. Pap., 51, 1475–1491, https://doi.org/10.1016/j.dsr.2004.06.011, 2004.

Waugh, D. W., Hall, T. M., Mcneil, B. I., Key, R., and Matear, R. J.: Anthropogenic CO2 in the oceans estimated using transit time distributions, Tellus B Chem. Phys. Meteorol., 58, 376–389, https://doi.org/10.1111/j.1600-0889.2006.00222.x, 2006.

Yool, A., Oschlies, A., Nurser, A. J. G., and Gruber, N.: A model-based assessment of the TrOCA approach for estimating anthropogenic carbon in the ocean, Biogeosciences, 7, 723–751, https://doi.org/10.5194/bg-7-723-2010, 2010.